HHS Public Access

Author manuscript

*Shock*. Author manuscript; available in PMC 2020 October 01.

Published in final edited form as:

*Shock*. 2019 October ; 52(4): 423–433. doi:10.1097/SHK.0000000000001280.

# Sphingosine-1-Phosphate Reduces Hemorrhagic Shock and Resuscitation-Induced Microvascular Leakage by Protecting Endothelial Mitochondrial Integrity

**Natascha G. Alves**, **Andrea N. Trujillo**, **Jerome W. Breslin**, **Sarah Y. Yuan**

Department of Molecular Pharmacology and Physiology, Morsani College of Medicine, University of South Florida, Tampa, FL

## Abstract

Excessive microvascular permeability is a serious complication following hemorrhagic shock and resuscitation (HSR). S1P has been shown to ameliorate microvascular leakage in a model of combined alcohol intoxication and hemorrhagic shock and resuscitation (HSR). In the current study, we tested the hypothesis that S1P reduces HSR-induced microvascular leakage by preserving endothelial cell junctional structure and the endothelial glycocalyx through protection of mitochondrial function. We used an established *in vivo* rat model of conscious HSR and assessed microvascular leakage, endothelial glycocalyx integrity, and mitochondrial function by intravital microscopy. Junctional integrity in the mesenteric microcirculation was assessed by confocal microscopy. Cultured rat intestinal microvascular endothelial cells monolayers were used to test the ability of S1P to protect against glycocalyx shedding and endothelial barrier dysfunction caused by direct disruption of mitochondrial integrity due to inhibition of mitochondrial complex III. The results show that *in vivo*, S1P protects against HSR-induced hyperpermeability, preserves the expression of adherens junctional proteins, and protects against glycocalyx degradation. S1P treatment during HSR also protects against mitochondrial membrane depolarization. S1P also protects against mitochondrial dysfunction-induced endothelial barrier dysfunction and glycocalyx degradation by acting through mitochondrial complex III. Taken together, our data indicate that S1P protects against HSR-induced mitochondrial dysfunction in endothelial cells, which in turn improves the structure of the endothelial glycocalyx after HSR and allows for better junctional integrity to prevention of excess microvascular permeability.

### Keywords

S1P; Hemorrhagic Shock; Endothelial barrier; Glycocalyx; Mitochondrial Function

Address to Correspondence: Jerome W. Breslin, PhD, Molecular Pharmacology and Physiology, University of South Florida, 12901 Bruce B Downs Blvd MDC8, Tampa, FL 33612, Tel (813) 974 7631, jbreslin@health.usf.edu.

CONFLICTS OF INTEREST AND SOURCES OF FUNDING

The authors have no conflicts of interest to declare. This work was supported by NIH grants R01HL098215, R01GM120774, R01GM097270, and R01HL070752. The content of this report is solely the responsibility of the authors and does not necessarily represent the official views of the National Institutes of Health.

## INTRODUCTION

Increased microvascular permeability to plasma proteins is a hallmark of traumatic injuries and sepsis, and is involved in the pathophysiology of diabetes, ischemia-reperfusion, and, cancer [1]. Failure to control the excessive extravasation of fluids and proteins results in edema, impairing normal tissue homeostasis. Hemorrhagic shock involves significant loss of intravascular volume that decreases tissue perfusion and leads to systemic microvascular hyperpermeability. If the extravasation of fluids is not readily resolved, the complications can culminate in multiple organ failure, which accounts for 50–60% of trauma related deaths. Fluid resuscitation following hemorrhage remains a major challenge, as initial resuscitation with standard care fluids may not improve patient outcome and may exacerbate endothelial damage [2].

Paracellular junctional proteins play a major role in controlling the endothelial barrier function in the microvasculature. VE-cadherin is an important adherens junctional protein that is connected to the actin cytoskeleton via association with catenins, particularly β-catenin. Dissociation of the VE-cadherin/β-catenin complex leads to increased microvascular permeability [3]. Early investigation on the effects of inflammatory mediators on barrier integrity suggested that increases in endothelial permeability were associated with changes in actin cytoskeleton organization and formation of paracellular gaps [4]. More recent studies using *in vitro* models of burn injury showed increased endothelial cell permeability and barrier disruption upon treatment with burn plasma. This was associated with actin stress fiber formation, loss of VE-cadherin/β-catenin complex from the cell periphery and gap formation in the paracellular cleft [5]. *In vivo* studies using models of hemorrhagic shock have shown increased permeability of the microvasculature, suggesting disruption of junctional proteins [6,7].

In addition to coordination between paracellular junctional proteins and the actin cytoskeleton, the endothelial glycocalyx layer (EGL) has also been elegantly demonstrated to be a modulator of microvascular permeability and immune cell-vessel wall interactions [8]. The EGL is a multilayer structure composed of glycosaminoglycan chains bound to proteoglycans and glycoproteins, that are associated extracellularly with the endothelial cell membrane [9]. Disruption of the glycocalyx during inflammatory processes exposes the endothelium to leukocyte adhesion, exacerbating the inflammation and leading to vascular pathology [8]. Shedding of glycocalyx components has been shown in both small and large animal models of hemorrhagic shock [10,11]. Moreover, severely injured trauma patients display glycocalyx degradation in association with increased microvascular permeability [12]. Studies aimed at diminishing microvascular permeability following hemorrhage found that resuscitation with fresh frozen plasma is able to restore and preserve the EGL, suggesting the involvement of plasma components in glycocalyx protection [13,14].

The mitochondrial content of endothelial cells is relatively modest. In rat endothelial cells, the mitochondria occupy only 2 – 6 % of the cell volume, in contrast to 28 % in hepatocytes and 32 % in cardiac myocytes [15]. Indeed, endothelial cells obtain a great portion of their energy from anaerobic glycolysis. Although the mitochondria are not the main source of energy production in endothelial cells, they do have important signaling roles in the vascular

endothelium [15]. Altered mitochondrial dynamics has been associated with endothelial dysfunction in patients with vascular diseases such as diabetes mellitus and atherosclerosis [15]. Activation of the mitochondrial intrinsic apoptotic signaling pathway has been suggested to play a role in HSR-induced hyperpermeability *in vivo* [6], and the mitochondrial complex III was shown to be involved in endothelial hyperpermeability [16].

Sphingosine-1-phosphate is an endogenous bioactive lipid synthesized by erythrocytes and platelets. S1P's function as a barrier enhancer has widely been demonstrated *in vitro*. Treatment of endothelial cells with S1P causes an increase in endothelial barrier function, and recruitment of junctional proteins such as VE-cadherin and β-catenin to intercellular junctions [17]. S1P has also been demonstrated to inhibit the degradation, and in fact stimulate, the synthesis of components of the glycocalyx such as heparan sulfate in endothelial cells [18]. Moreover, S1P's contribution to the maintenance of vascular permeability in isolated microvessels is associated to preservation of the glycocalyx [19]. *In vivo*, intravenous administration of S1P reduces inflammation and edema formation in LPS-induced microvascular leakage models [20].

In our previous study, we demonstrated that administration of S1P during resuscitation following combined alcohol intoxication and hemorrhage ameliorated microvascular leakage in rat mesenteric microvessels and alleviated hypotension after shock [7]. However, we did not investigate the mechanisms of S1P-induced protection of barrier function during hemorrhagic shock and resuscitation (HSR). Therefore, the objective of the current study was to assess how S1P protects the structure and function of the microvascular endothelium during HSR. We hypothesized that S1P improves microvascular barrier function during HSR by preserving the paracellular junctions, preventing loss of the glycocalyx layer, and protecting endothelial cells from damage induced by mitochondrial dysfunction.

## MATERIALS AND METHODS

### Cells and Reagents

Rat Primary Intestinal Mesenteric Vascular Endothelial Cells (RIMEC) and complete rat endothelial cell medium (ECM) were purchased from Cell Biologics (Chicago, IL). JC-1, a mitochondrial membrane potential sensor, polyclonal rabbit anti-VE-cadherin (CD144), and all fluorescence-labeled secondary antibodies were obtained from Invitrogen (Carlsbad, CA). Mouse anti-β-catenin monoclonal antibody (L54E2) was purchased from Cell Signaling Technology (Boston, MA). The mouse monoclonal anti-heparan sulfate antibody (F58–10E4) was obtained from Amsbio (Cambridge, MA). Mouse anti-β-actin (C4) horseradish peroxidase-conjugated was from Santa Cruz Biotechnology, Inc. (Santa Cruz, CA). Sphingosine-1-phosphate was obtained from Tocris Biotechne (Minneapolis, MN). Fluorescein isothiocyanate (FITC)-conjugated albumin and FITC-dextran were purchased from Sigma-Aldrich (St. Louis, MO). Antimycin-A and the rabbit anti-Caveolin-1 polyclonal antibody (aa 1–17) were from Abcam (Cambridge, MA). Lactated Ringers and 0.9% sodium chloride solutions were obtained from Henry Schein (Ocala, FL). All other reagents were obtained from Sigma-Aldrich unless otherwise specified.

## Animals

This study was approved by the University of South Florida Institutional Animal Care and Use Committee (permit number IS00005044) and performed in accordance with the U.S. Animal Welfare Act, U.S. Public Health Service Policy on the Humane Care and Use of Laboratory Animals and the National Institutes of Health *Guide for Care and Use of Laboratory Animals.* 12–15 week old male Sprague-Dawley rats (330 – 355 g) were purchased from Envigo (Indianapolis, IL) and housed in a controlled environment (22 °C, 12h light/12h dark cycle) in the vivarium, and provided a standard diet (Purina Rat Chow, Ralston Purina) and water *ad libitum* for a one-week acclimation period prior to surgery. All animals were humanely euthanized with Somnasol Euthanasia-III Solution (87 mg/kg i.v., Henry Schein, Dublin, OH) following experimental protocols.

## Surgical Preparation

The surgical procedures for this model have been recently described in detail by our lab and others [7,21]. Briefly, the rats were anesthetized with isoflurane, an incision on the ventral side of the neck was made, and sterile catheters flushed with 0.9% sterile sodium chloride USP (Baxter, Deerfield, IL) were implanted in the left common carotid artery and the right external jugular vein. Catheters were secured with a purse-string suture, thermally sealed, subcutaneously routed to the dorsal nape of the neck and exteriorized through an incision. The catheters were secured to the closed incision with suture, coiled and wrapped with masking tape to prevent the rat from accessing it. Carprofen (5 mg/kg subcutaneously; Putney, Portland, ME) was administered every 12h for the first 48h following surgery to minimize pain during recovery. Before experiments, animals were allowed to recover for 5 to 7 days in the same conditions as the acclimation period.

## Fixed-pressure Hemorrhagic Shock and Resuscitation Protocol

After 5 to 7 days of post-surgery recovery period, rats were subjected to a fixed-pressure hemorrhagic shock and resuscitation (HSR) protocol while conscious and unrestrained, as previously described [7,21]. A fixed-pressure hemorrhage model was chosen over a fixed-volume model because constant-pressure models are more reliable for experimental standardization and reproducibility [21]. With this method, we can reliably evaluate the physiological changes in our tissue of interest that occur during a specific central pressure. Moreover, we use conscious, unrestrained rats because handling, restraint and anesthetics all significantly impact blood pressure [7]. The experimental groups were Sham control rats, HSR, and HSR + S1P. The Sham control group received the same catheter implantation surgical procedure but did not undergo the HSR protocol. Briefly, the rats were placed in small cages and the catheters were routed through the top of each cage. The carotid catheter was connected to a pressure transducer (ADInstruments PowerLab 4/35 with Quad Bridge amplifier system and LabChart software, ADInstruments, Colorado Springs, CO) for continuous blood pressure recording and monitoring throughout the whole protocol. The rats were allowed to acclimate by roaming freely in the cage for 60 minutes before the start of hemorrhage. At the beginning of hemorrhage, arterial blood was withdrawn from the carotid catheter (blood pressure recording is momentarily interrupted at this point) to achieve a blood pressure of 50–60 mmHg, which is maintained for 60 minutes. If necessary, additional

blood was withdrawn during this period to maintain the blood pressure. At the end of the hemorrhage period, warm resuscitation solution (Lactated Ringer's) was delivered intravenously through the jugular catheter as an initial bolus with a volume of 40% of the total blood volume removed (TBR) followed by an infusion of 2 X TBR over 60 minutes. For the HSR + S1P group, S1P was dissolved in the resuscitation fluid at a dose of 0.1 mg/kg. Our previous findings demonstrated that this dose is most effective to protect against microvascular permeability induced by combined acute alcohol intoxication and HSR [7]. The HSR group received warm lactated ringers without S1P for resuscitation.

### Intravital Microscopy and In vivo Assessment of Microvascular Permeability

Following the HSR protocol, microvascular leakage of the mesenteric microcirculation was assessed by intravital microscopy (IVM) as previously described [7,21] Briefly, rats were anesthetized with isoflurane (4% induction, 2% maintenance), the ventral abdominal fur was shaved and the skin was sterilized with 4% chlorohexidine gluconate solution (CareFusion, Leawood, KS), 100% ethyl alcohol, and 7.5% Povidone-iodine (Purdue Products L.P., Stamford, CT). Next, a midline laparotomy was performed, and a section of the small intestine was exteriorized, spread out over an optical stage and superfused with warm Ringer's solution. The animal's body temperature was maintained using a heating plate placed under the rat's body and monitored by a rectal thermometer. For assessing microvascular leakage, FITC-conjugated albumin dissolved in Lactated Ringer's solution was administered intravenously through the jugular catheter as a 1 ml bolus (100 mg/kg) followed by continuous infusion (0.15 mg/kg/min). Observation of mesenteric microvessels was done with a fluorescent microscope (Nikon Eclipse E600) using a 10X objective (Nikon Instruments Inc., Natick, MA) at 488 nm excitation. Fluorescent images were captured via Photometrics HQ2 digital camera (Photometrics, Tucson, AZ), controlled by Micromanager software. Analysis of FITC-albumin extravasation was done with ImageJ, by measuring the integrated optical intensity (IOI) of extravascular areas close to post-capillary venules [21].

### Immunofluorescence Labeling and Confocal Microscopy

For some experiments, immunofluorescence confocal microscopy of the junctional protein VE-cadherin on small intestine mesenteric windows was performed following the HSR protocol. At the end of the resuscitation period, the rats were anesthetized with isoflurane, a small laparotomy was performed, and the small intestine and mesentery were harvested and rinsed in ice-cold albumin-physiological salt solution (APSS; 120 mM NaCl, 4.7 mM KCl, 2 mM $CaCl_2{\cdot}2H_2O$, 1.2 mM $MgSO_4{\cdot}7H_2O$, 1.2 mM $NaH_2PO_4$, 2 mM Na pyruvate, 5 mM glucose, 0.02 mM EDTA, 3 mM MOPS, and 1% BSA). Rats were then immediately euthanized. A section of the mesentery was pinned in a dissection dish containing ice-cold APSS and, with the aid of a dissection microscope, mesenteric windows were carefully dissected from the surrounding tissue. Each window was fixed with 4% paraformaldehyde for 15 minutes at room temperature, washed twice with 100 mM glycine buffer to quench the fixation, and then washed once with $Ca^{2+}$/$Mg^{2+}$-free Dulbecco's PBS (DPBS). Windows were then permeabilized with 0.1% TritonX-100 in 1X PBS for 30 minutes and washed three times with DPBS for 5 minutes to remove the TritonX-100 detergent. After permeabilization, windows were blocked in 5% donkey serum in DPBS for 45 to 60 minutes, and then incubated overnight at 4 °C with VE-cadherin primary antibody (1:400)

diluted in antibody buffer (151 mM NaCl, 17 mM trisodium citrate, 2% donkey serum, 1% BSA, 0.05% Triton X-100, and 0.02% $NaN_3$). After overnight incubation with primary antibody, the mesenteric windows were rinsed (four times for 10 min) with an antibody wash solution (151 mM NaCl, 17 mM trisodium citrate, and 0.05% Triton X-100) and then incubated with secondary antibody (1:500-diluted AlexaFluor-488 donkey anti-rabbit IgG) diluted in antibody buffer for 60 min at room temperature, followed by four rinses of 10 min in antibody wash solution. After the last wash, each window was splayed on a glass slide with a SecureSeal imaging spacer and 20 μl of 50% glycerol and covered with a glass coverslip. Confocal image stacks (0.5 – 1 μm z sections) of the microvessels in each window were taken with an Olympus FV1200 spectral inverted laser scanning confocal microscope with 40X objective at the Lisa Muma Weitz Advanced Microscopy and Cell Imaging Core at the University of South Florida. The images were analyzed using Imaris image analysis software (Bitplane, Concord, MA). The confocal image stacks were processed into maximum intensity z-projections for presentation as figures using ImageJ software.

## Western Blotting

Following the experimental protocol for each group, some rats were used for protein expression analysis of the mesenteric microvasculature. Briefly, at the end of the experiment, the rats were humanely euthanized and the small intestine and mesentery was excised and immediately placed in a beaker containing ice-cold APSS. The tissue was splayed on a dissecting dish and the mesenteric microvasculature was carefully dissected away from the surrounding tissue, as previously described [6]. For total protein extraction, the microvasculature was homogenized in RIPA lysis buffer containing protease inhibitors (Thermo Fisher, Rockford, IL). Tissue homogenates were centrifuged for 15 min at 14,000 rpm at 4 °C, and the supernatant was collected for protein concentration estimation using Pierce's bicinchoninic acid assay (BCA) assay kit (Thermo Fisher). Each sample consisted of microvessels pooled from 7 – 10 rats per experimental group. To extract the cytosolic protein fraction, the microvessels were dissected as described above, and a plasma membrane protein extraction kit (Abcam, Cambridge, MA) was used according to the manufacturer's protocol to extract the membrane and cytosolic protein fractions. Our samples yielded concentrations sufficient for immunodetection of proteins in the total and cytosolic fractions, but not in the membrane fraction by Western blot. The protein samples were heated at 100 °C for 5 minutes and subjected to SDS-PAGE, then transferred to PVDF membranes. The membranes were blocked for 1 hour at room temperature with 5% bovine serum albumin (BSA) in Tris-buffered saline solution with 0.1% Tween-20 (TBS-T) and were incubated with mouse anti-β-catenin (1:300), rabbit anti-Caveolin-1 (1.5 μg/ml) or HRP-conjugated anti-β-actin (1:1000) diluted in blocking solution overnight at 4 °C. The membranes were washed three times with TBS-T. For the membranes incubated with the anti-β-catenin and anti-caveolin-1 antibodies, an additional incubation with HRP-conjugated-anti-mouse or anti-rabbit IgG secondary antibodies (1:1000) was performed at room temperature for 1 h. Following three washes with TBST-T, the protein bands were visualized using the SuperSignal West Pico Chemiluminescent Substrate kit (Thermo Fisher, Rockford, IL) and the Chemidoc XRS+ Molecular Imager with Image Lab software (Bio-Rad, Hercules, CA). Bands were quantified using ImageJ software. Cytosolic β-catenin

bands were normalized to their respective cytosolic actin levels for comparison between groups.

### In vivo Measurements of Glycocalyx Thickness and Integrity

We assessed the integrity of the endothelial surface glycocalyx layer (EGL) in Sham control, HSR and HSR + S1P rats by direct visualization using *Bandeiraea simplicifolia* (BSI)-lectin conjugated to FITC (FITC-lectin; Sigma-Aldrich, St. Louis, MO), which has high specificity for sugar moieties and can bind to the polysaccharide side chains that compose the EGL [22]. Following the experimental procedure, rats were prepared for IVM as described above. Once an area with good blood flow was detected, we administered FITC-lectin (6.25 mg/kg diluted in 1 ml saline) via the jugular catheter and allowed for systemic distribution before images were taken using the 10x objective at 488 nm excitation. At least three post-capillary venules were used for quantification of the EGL in each rat. All vessels were comparable in blood flow and diameter. The endothelial surface glycan concentration was quantified in ImageJ software by manually tracing a measurement path along the wall of each vessel, then averaging the radial intensity distribution on each pixel along the path, as previously described [23].

Additionally, we used the dye-exclusion method [24,25] to estimate the thickness of the glycocalyx. After preparing each rat for IVM, a bolus of FITC-labeled dextran (150 kDa) was administered via jugular catheter, and fluorescence was allowed to reach a steady level. Post-capillary venules with steady blood flow were selected, and both brightfield and fluorescent images were captured with a 10X objective. Large-size molecules such as 150 kDa dextrans are excluded from the vessel wall by the glycocalyx, so the difference in vascular widths between brightfield and fluorescence images represents the thickness of the glycocalyx [25]. Images were analyzed using ImageJ software.

### Leukocyte-Endothelium Rolling and Adhesion

Leukocyte rolling and adhesion were analyzed by IVM in Sham, HSR and HSR + S1P rats following the experimental protocol. Rats were prepared for IVM and mesenteric venules (30 – 60 μm diameter) with comparable blood flow were selected for visualization of leukocyte dynamics. The exteriorized mesentery was continuously superfused with 37 °C Ringer's solution. The microcirculation was observed using a Nikon Eclipse E600 microscope and 10X objective, and rapid time-lapse brightfield image sets were acquired over a 30-s period. The microscope was focused above and below the diametral plane. Rolling and adhesion were measured by assessing the frame-by-frame playback of the digital image set for individual leukocytes. The number of leukocytes that were rolling in a velocity noticeably slower than that of cells in the central blood stream was counted for each selected vessel segment. A leukocyte was defined adherent if it remained stationary for at least 5 s. Leukocyte rolling and adhesion are expressed as the number of leukocytes per 100 μm of vessel length as previously described [26].

### In vivo Assessment of Mitochondrial Transmembrane Potential

Following the HSR protocol, some rats were prepared for *in vivo* visualization of mitochondrial transmembrane potential of mesenteric microvessels using IVM. Once

animals had a section of their small intestine and mesentery exposed, they were placed on an optical stage and the mesenteric vasculature was superfused with warm JC-1 (10 μg/ml in sterile 0.9% saline). Before image capture, the JC-1 was rinsed off the mesentery. JC-1 exhibits potential-dependent accumulation within mitochondria and its response is specific to depolarization [27]. JC-1 is able to enter the matrix of healthy mitochondria, where it accumulates and forms aggregates that fluoresce red. Upon depolarization, the mitochondrial potential collapses and JC-1 cannot accumulate, remaining in the cytoplasm as a monomeric green fluorescent form [6]. Consequently, a decrease in the red/green fluorescence intensity ratio indicates mitochondrial depolarization. Images were captured with a 20x objective, by exciting both the monomer and the J-aggregate at 488 nm, and detecting green and red emission at 530 and 590 nm wavelengths. At least three post-capillary venules were selected for analysis in each rat. Images were analyzed for changes in mitochondrial membrane potential by determining the red/green fluorescence intensity ratio in the walls of these venules using ImageJ.

### In vitro assessment of mitochondrial membrane potential

Rat Primary Intestinal Mesenteric Vascular Endothelial Cells (RIMEC) were grown to confluence in complete endothelial cell medium (ECM) containing 2% fetal bovine serum (FBS) at 37 °C and 5% $CO_2$. For live-cell imaging of mitochondrial function, the cells were seeded onto glass-bottom dishes pre-coated with 0.2 % gelatin and allowed to mature for 3 to 5 days post confluence. On the day of the experiment the medium was changed to warm basal endothelial cell medium (bECM) containing JC-1 (2 μg/ml) and allowed to stabilize at 37 °C for 15 min. The dye-containing medium was washed off with basal medium and the cells were randomized into groups that were treated with bECM (controls), bECM containing antimycin-A (10 μM final concentration), or treated with antimycin-A followed by S1P treatment (1 μM final concentration). At 10 min post-treatment, images were captured with a Olympus FV1200 spectral inverted laser scanning confocal microscope using a 40X objective, by exciting JC-1 monomer at 488 nm and selectively exciting the J-aggregate at 554 nm, and detecting green and red emissions at 530 and 590 nm. ImageJ software was used to estimate the red/green fluorescence ratio from the captured confocal images in at least 4 cells in each experiment.

### Transendothelial Electrical Resistance

RIMEC were grown to confluence in complete endothelial cell medium (ECM) (containing 2% fetal bovine serum (FBS) at 37 °C and 5% $CO_2$. Cells were seeded onto gold electrode arrays pre-coated with 0.2% gelatin for assessment of transendothelial electrical resistance (TER) using an electric cell-substrate impedance sensor (ECIS; Applied Biophysics, Troy, NY). The ECIS system is a well-established indicator of endothelial barrier function based on the tightness of cell-cell junctions [26]. Cells were allowed to grow at 37 °C for 3 – 5 days post-confluence before experiments to allow for maturation of paracellular junctions, with medium changed every other day. On the day of the experiment, the medium was changed to basal endothelial cell medium (bECM) 1 h before the start of the experiment, and the arrays were attached to the ECIS system. A 1 μA AC signal at 4 kHz was applied through a 1-MΩ resistor to a constant-current source, and the in-phase and out-of-phase voltage, respectively proportional to resistance and capacitance, were recorded with the

ECIS software. The data are expressed as TER normalized to the 0-min time-point. Vehicle (bECM) or antimycin-A (10 μM) were added at time = 0, immediately followed (~1 min later) by addition of S1P (1 μM) or vehicle, and the TER was recorded for 10 hours to determine changes in barrier function over time.

### In vitro Immunofluorescence of Endothelial Glycocalyx

RIMEC were grown at 37 °C and 5 % $CO_2$ as described above. For assessment of glycocalyx integrity, cells were seeded onto glass coverslips pre-coated with 0.2 % gelatin and allowed to mature for 3 days post confluence. Medium was changed every other day. On the day of the experiment, the medium was changed to 37 °C bECM 30 minutes before treatment. Cells were treated with either vehicle (bECM) or antimycin-A (10 μM) or antimycin-A followed by treatment with S1P (1 μM) for 1 hour. Following treatment, cells were washed once with DPBS and fixed with 2% paraformaldehyde (PFA) and 0.1 % glutaraldehyde solution in DPBS for 30 min. After fixation, PFA was rinsed with DPBS and cells were blocked with 2 % donkey serum in DPBS for 1 hour. Cells were incubated with mouse monoclonal anti-heparan-sulfate antibody overnight at 4 °C. Three washes of 10 min each were done with DPBS, followed by incubation with secondary donkey anti-mouse antibody conjugated to Alexa Fluor 488 for 1 hour at room temperature. After three washes of 10 min with DPBS, the coverslips were mounted onto slides with Prolong Gold antifade reagent with DAPI (Invitrogen, Carlsbad, CA). Confocal images were taken with an Olympus FV1200 spectral inverted laser scanning confocal microscope with a 60X objective at the Lisa Muma Weitz Advanced Microscopy and Cell Imaging Core at the University of South Florida. The image stacks were processed and analyzed using ImageJ.

### Data Analyses

All summarized data are presented as mean ± S.E. Statistical analyses and preparation of graphs for presentation were performed using Prism 6 (GraphPad Software, LaJolla, CA). When only two groups were compared, an unpaired t-test was utilized. To compare treatments over time, repeated-measures ANOVA was used, followed by Fisher's LSD test to compare individual time points, unless otherwise specified. For comparison of three or more groups, one-way ANOVA was used, followed by Tukey's test to perform multiple comparisons. Significance was accepted at $P<0.05$. For the studies with rats, values of N in each figure represent the number of rats studied with the exception of Western blots, in which samples from multiple rats had to be pooled to obtain sufficient protein. For *in vitro* experiments, N represents the number of trials, with each trial consisting of groups composed of multiple endothelial cells or monolayers studied as indicated in the figure legends.

## RESULTS

### Mean Arterial Blood Pressure and FITC-Albumin Extravasation

To evaluate how S1P impacts HSR-induced hypotension and microvascular leakage following HSR, we monitored the mean arterial blood pressure (MAP) throughout the protocol and assessed FITC-albumin extravasation by IVM. Administration of S1P in the resuscitation fluids (lactated Ringer's solution) significantly raised MAP at the end of the

resuscitation period, compared to rats that received lactated Ringer's only (Fig. 1A). When examining microvascular leakage, in time-matched Sham rats, the FITC-albumin remained in the luminal compartment of the microvessels, with minimal fluorescence intensity in the extravascular space. HSR rats showed high levels of fluorescence in the areas surrounding the mesenteric microvasculature. Rats that received S1P in their resuscitation fluid had relatively low fluorescence outside the vasculature (Fig. 1B). Quantification of these data showed that the HSR group had a significantly higher mean integrated optical intensity (IOI) in the extravascular areas near the microvessels compared to sham controls, indicating elevated microvascular leakage of FITC-albumin. HSR rats that received S1P (HSR + S1P) had significantly lower IOI compared to HSR rats (Fig. 1C). These data suggest that the S1P improves mean arterial pressure after hemorrhage, and attenuates the microvascular hyperpermeability induced by HSR, thus preventing loss of central fluid volume.

## Paracellular Junction Protein Integrity

Because the expression and localization of junctional proteins such as VE-cadherin at the paracellular junctions is pivotal for endothelial barrier functional integrity, we performed immunofluorescence confocal microscopy of mesenteric post-capillary venules to determine to what extent S1P may reduce HSR-induced microvascular leakage by improving junctional location of VE-cadherin. Fig. 2 shows that VE-cadherin is localized between endothelial cells in Sham rats, outlining a clear boundary for each endothelial cell. HSR disrupted the localization of VE-cadherin, and also significantly decreased the intensity of labeling. HSR + S1P rats showed high localization of VE-cadherin at the junctions, and significantly higher VE-cadherin expression compared to HSR rats (Fig. 2A, B).

The adherens junction protein β-catenin is known to stabilize VE-cadherin and aid in paracellular junction maturation and function. Dissociation of β-catenin from VE-cadherin and its translocation to the cytosol has been demonstrated previously in cultured endothelial cells treated with activated neutrophils or with plasma from rats that have undergone burn injury [3,5,28]. Therefore, we investigated its total and cytosolic expression following HSR and S1P treatment in lysates of isolated microvessels pooled from multiple rats in each group. Our experiments showed no change in the total expression of β-catenin in mesenteric microvessels of sham, HSR or HSR + S1P rats. However, we observed a noticeable increase in the cytosolic levels of β-catenin following HSR compared to Sham rats. HSR + S1P rats had significantly lower cytosolic levels of β-catenin compared to HSR rats (Fig. 2C, D ). To verify cytosolic protein fraction isolation, we also performed Western blots for caveolin-1, a protein known to be localized to lipid rafts of the plasma membrane, where it performs several roles in membrane dynamics [29]. The band intensities for caveolin-1 were lower in the cytosolic fraction than those for the total protein fraction of all three groups, indicating successful fractionation. Interestingly, higher cytosolic levels of caveolin-1 in the HSR group were observed and might indicate its dissociation from membrane caveolae as a response to injury. Given that total β-catenin expression did not change, this data suggests that HSR causes a shift in β-catenin localization from the junctions to the cytosol, destabilizing VE-cadherin and contributing for the increase in permeability. Treatment with S1P seems to recruit the available β-catenin in the cytosol back to the paracellular junctions during HSR, and this might be contributing to rescue albumin permeability.

### S1P-mediated Protection of Endothelial Glycocalyx Layer

Hemorrhagic shock and resuscitation has been shown to cause degradation of the endothelial glycocalyx layer (EGL) [13]. In the current study, we found that HSR caused a significant drop in the concentration of FITC-lectin bound to the walls of post-capillary venules compared to Sham rats (Fig. 3). Rats that received S1P in the resuscitation fluid (HSR + S1P) had significantly higher FITC-lectin fluorescence compared to HSR rats (Fig. 3A, B). We also measured the thickness of the glycocalyx in the mesenteric post-capillary venules by using the dye-exclusion method. We found that rats subjected to hemorrhage and resuscitation without S1P had significant reduction in glycocalyx thickness compared to Sham rats. Rats that received S1P resuscitation displayed significantly thicker glycocalyx compared to HSR rats (Fig. 3C, D). These data suggest that S1P's barrier-protective effects during HSR are partly due to its ability to maintain glycocalyx integrity.

### Leukocyte-endothelium Dynamics

Degradation of the glycocalyx plays a role in inducing a pro-inflammatory response and promoting leukocyte adhesion to endothelial cells [8]. Therefore, as an indirect indicator of glycocalyx integrity, we evaluated leukocyte interaction with the endothelium of mesenteric post-capillary venules in Sham, HSR, and HSR + S1P rats. All venules chosen were comparable to flow rate and diameter. Leukocyte rolling and adhesion data are shown in Fig. 4. Treatment with S1P resulted in significantly lower number of slow-rolling leukocytes in mesenteric venules after HSR compared to HSR rats that did not receive S1P (Fig. 4A). HSR rats exhibited significantly greater leukocyte adhesion (leukocytes that were stationary for 5 seconds or more) to the endothelium compared to Sham rats. This effect was reversed by resuscitation with S1P (Fig. 4B).

### Mitochondrial Transmembrane Potential and Endothelial Barrier Function

Previous studies have reported that changes in mitochondrial function in response to HSR could be associated with microvascular hyperpermeability [6] In order to assess the effects of S1P in mitochondrial function of mesenteric microvessels in the context of HSR, we used intravital observation of microvessels loaded with the mitochondrial membrane potential sensor JC-1. In cells with healthy mitochondria, JC-1 exists as a monomeric form in the cytosol (green fluorescence) and also accumulates in the mitochondria, fluorescing red. Upon depolarization, JC-1 cannot accumulate in the mitochondria and produces only green fluorescence [6]. Mitochondrial depolarization is seen as a decrease in the red to green fluorescence ratio. We found that HSR caused mitochondrial depolarization in mesenteric postcapillary venules, as seen as a significant decrease in red/green ratio when compared to sham rats (Fig. 5). Treatment with S1P during resuscitation protected mitochondrial membrane potential and reversed the effect of HSR, significantly increasing red/green fluorescence ratio (Fig. 5).

To directly test whether mitochondrial depolarization increases impairs the endothelial barrier, we treated cultured rat intestinal mesenteric endothelial cells (RIMEC) with antimycin-A (AA), an inhibitor of mitochondrial respiratory chain complex III that has been previously been associated with endothelial monolayer permeability [16]. Fig. 6A shows a time course of changes in TER, an index of endothelial barrier function, for RIMEC treated

with vehicle alone (control), AA + Vehicle or AA + S1P. AA treatment immediately caused the TER to begin to drop and the reduction in TER was sustained throughout the time course. For the cells treated with S1P given just after the addition of AA, only a small drop in TER occurred, which was insignificant compared to control (Fig. 6A), indicating that S1P is able to protect RIMEC from AA-induced barrier dysfunction.

### Mitochondrial Complex III Inhibition and Glycocalyx Integrity

In order to assess whether the complex III inhibition causes degradation of the endothelial glycocalyx layer (EGL), we treated cells with AA and evaluated surface expression of the glycosaminoglycan heparan sulfate (Fig. 6). We found that treatment with AA degraded heparan sulfate surface expression on cultured RIMEC (Fig. 6B, C). Treatment with S1P after AA preserved the surface expression of heparan sulfate (Fig. 6B, C). These results suggest that normal mitochondrial complex III activity, and by extension normal mitochondrial membrane integrity, are required for normal maintenance of the EGL, and show that S1P has the potential to attenuate EGL shedding caused by mitochondrial dysfunction during inhibition of mitochondrial complex III.

### In vitro Mitochondrial Depolarization

In order to support our *in vivo* findings that S1P protects mitochondrial function by blocking mitochondrial depolarization, we performed imaging of live RIMEC loaded with JC-1 and treated with antimycin-A in the absence or presence of S1P (Fig. 7). We found that inhibition of complex III with AA caused depolarization of the mitochondria in RIMEC monolayers, and that treatment with S1P after AA was able to rescue this effect (Fig. 7). This result shows that S1P-induced protection of mitochondrial function is due its ability to protect against inhibition of mitochondrial respiratory chain complex III.

## DISCUSSION

The complications that arise from fluid resuscitation following hemorrhagic shock remain a serious problem, including resuscitation-related changes in endothelial cell function and loss of endothelial integrity, contributing to microvascular leakage and edema formation [7]. In the current study, we demonstrate that S1P protects against microvascular leakage and improves blood pressure when administered during resuscitation following hemorrhagic shock. We also show that resuscitation with S1P prevents HSR-induced disruption of endothelial junctions and the glycocalyx layer. Likewise, rolling and adhesion of leukocytes, which can be facilitated by glycocalyx shedding, are also attenuated with S1P treatment. Furthermore, our data show for the first time that S1P can inhibit HSR-induced disruption of endothelial mitochondrial membrane potential. Lastly, we provide novel evidence that mitochondrial complex III inhibition can cause endothelial barrier dysfunction. S1P can restore barrier integrity and prevent shedding of the glycocalyx in the presence of mitochondrial complex III inhibition. Collectively, the data suggest that S1P ameliorates HSR-induced microvascular leakage at least in part through its ability to attenuate mitochondrial membrane disruption.

Our findings that S1P can ameliorate HSR-induced hypotension and microvascular leakage are in agreement with previous work utilizing administration of S1P or its analog FTY720 in resuscitation fluids [7,30]. The mechanisms involved in S1P-mediated reduction of microvascular leakage are not completely understood, but involve activation of one or more S1P receptors, followed by rapid activation of Rho family small GTPases, changes in the cytoskeleton including increased protrusion of local lamellipodia, plus changes in junctional and focal adhesions [31–33]. In addition, S1P also has been shown to promote glycocalyx integrity in cultured endothelial cells [18,19]. As nearly all of the mechanistic studies have been performed in cultured cells, our current findings provide novel *in vivo* evidence that S1P is effective at preventing HSR-induced disruption of VE-cadherin localization at endothelial junction in combination with preserving glycocalyx integrity.

Consistent with previous reports [6], we show that HSR causes a disruption in mitochondrial transmembrane potential in mesenteric venules. In addition, we provide the novel finding that S1P administration in the resuscitation fluid attenuates the HSR-induced disruption of mitochondrial membrane integrity. To determine whether protection of mitochondrial membrane potential may mediate S1P-induced attenuation of microvascular leakage caused by HSR, we utilized a cultured RIMEC model in which we could study the direct impact of mitochondrial disruption on barrier function. The results demonstrate that mitochondrial depolarization as a result of mitochondrial complex III inhibition with AA can directly cause endothelial barrier dysfunction. These results support previous reports that complex III is indeed involved in endothelial cell hyperpermeability [16]. We also show that inhibition of complex III causes the degradation of components of the glycocalyx. Direct disruption of the glycocalyx has previously been shown to increase endothelial permeability [18]. We also present the novel finding that treatment with S1P partially restores the AA-induced loss of mitochondrial membrane potential, in combination with prevention of 1) AA-induced shedding of the glycocalyx component heparan sulfate, and 2) AA-induced barrier dysfunction. Collectively, the current results, in context with the previous literature, suggest that S1P-induced enhancement of endothelial barrier function is due at least in part to stabilization of mitochondrial membrane potential, which in turn promotes glycocalyx integrity. These results also show that S1P can protect the mitochondrial membrane from disruptions of the mitochondrial transport chain at the level of Complex III.

While our current study focused on the ability of S1P to rescue microvascular permeability increases caused by HSR, in a previous investigation we observed that S1P confers a similar benefit when HSR is combined with acute alcohol intoxication [7]. Under such conditions, alcohol appears to act by causing additional insult to the endothelial barrier. For example, paracellular junction integrity would likely be further disrupted with alcohol treatment preceding HSR. This is supported by studies showing decreased expression of tight junction proteins claudin-5, occludin and ZO-1 upon treatment of brain microvascular endothelial cells with alcohol, which was accompanied by a decrease in barrier function [34]. In addition, our laboratory recently reported that S1P rescues barrier function of brain microvascular endothelial cell monolayers in which barrier integrity has been disrupted by alcohol. Enhanced localization of β-catenin, VE-cadherin and Claudin-5 at endothelial junctions accompanied the recovery of barrier function [35]. These data suggest that some

common mechanisms probably underlie the ability of S1P to enhance the endothelial barrier whether hyperpermeability is caused by HSR or alcohol.

In summary, our findings present the first demonstration that S1P can protect against HSR-induced endothelial mitochondrial membrane disruption in combination with endothelial junctional and glycocalyx damage, increased leukocyte rolling and adhesion, and microvascular leakage. Our findings provide new insights about the importance of endothelial mitochondrial function as a potential pharmacologic target for future therapeutic interventions. We expect that future work investigating the mechanism that explains how mitochondrial function contributes to the integrity of the endothelial glycocalyx and intercellular junctions will produce additional advances that may lead to improved therapeutics to prevent excessive microvascular leakage in trauma patients.

## REFERENCES


1. Yuan SY, Breslin JW, Perrin R, Gaudreault N, Guo M, Kargozaran H, Wu MH. Microvascular permeability in diabetes and insulin resistance. Microcirculation 14: 363–373, 2007. [PubMed: 17613808]
2. Dewar D, Moore FA, Moore EE, Balogh Z. Postinjury multiple organ failure. Injury 40: 912–918, 2009. [PubMed: 19541301]
3. Guo M, Breslin JW, Wu MH, Gottardi CJ, Yuan SY. VE-cadherin and beta-catenin binding dynamics during histamine-induced endothelial hyperpermeability. Am J Physiol Cell Physiol 294: C977–984, 2008. [PubMed: 18287330]
4. Thurston G, Baldwin AL, Wilson LM. Changes in endothelial actin cytoskeleton at leakage sites in the rat mesenteric microvasculature. Am J Physiol 268: H316–329, 1995. [PubMed: 7840278]
5. Tinsley JH, Breslin JW, Teasdale NR, Yuan SY. PKC-dependent, burn-induced adherens junction reorganization and barrier dysfunction in pulmonary microvascular endothelial cells. Am J Physiol Lung Cell Mol Physiol 289: L217–223, 2005. [PubMed: 15821015]
6. Childs EW, Tharakan B, Hunter FA, Tinsley JH, Cao X. Apoptotic signaling induces hyperpermeability following hemorrhagic shock. Am J Physiol Heart Circ Physiol 292: H3179–3189, 2007. [PubMed: 17307990]
7. Doggett TM, Alves NG, Yuan SY, Breslin JW. Sphingosine-1-Phosphate Treatment Can Ameliorate Microvascular Leakage Caused by Combined Alcohol Intoxication and Hemorrhagic Shock. *Sci Rep* 7: 4078, 2017. [PubMed: 28642485]
8. Becker BF, Chappell D, Jacob M. Endothelial glycocalyx and coronary vascular permeability: the fringe benefit. Basic Res Cardiol 105: 687–701, 2010. [PubMed: 20859744]
9. Curry F, Adamson R. Endothelial glycocalyx: permeability barrier and mechanosensor. Ann Biomed Eng 40: 828–839, 2012. [PubMed: 22009311]
10. Peng Z, Pati S, Potter D, Brown R, Holcomb JB, Grill R, Wataha K, Park PW, Xue H, Kozar RA. Fresh frozen plasma lessens pulmonary endothelial inflammation and hyperpermeability after hemorrhagic shock and is associated with loss of syndecan 1. Shock 40: 195–202, 2013. [PubMed: 23807246]
11. Smart L, Boyd CJ, Claus MA, Bosio E, Hosgood G, Raisis A. Large-Volume Crystalloid Fluid Is Associated with Increased Hyaluronan Shedding and Inflammation in a Canine Hemorrhagic Shock Model. Inflammation 41: 1515–1523, 2018. [PubMed: 29728805]
12. Rahbar E, Cardenas JC, Baimukanova G, Usadi B, Bruhn R, Pati S, Ostrowski SR, Johansson PI, Holcomb JB, Wade CE. Endothelial glycocalyx shedding and vascular permeability in severely injured trauma patients. J Transl Med 13: 117, 2015. [PubMed: 25889764]
13. Torres LN, Chung KK, Salgado CL, Dubick MA, Torres Filho IP. Low-volume resuscitation with normal saline is associated with microvascular endothelial dysfunction after hemorrhage in rats, compared to colloids and balanced crystalloids. Crit Care 21: 160, 2017. [PubMed: 28659186]

14. Torres LN, Sondeen JL, Dubick MA, Filho IT. Systemic and microvascular effects of resuscitation with blood products after severe hemorrhage in rats. J Trauma Acute Care Surg 77: 716–723, 2014. [PubMed: 25494423]
15. Tang X, Luo YX, Chen HZ, Liu DP. Mitochondria, endothelial cell function, and vascular diseases. Front Physiol 5: 175, 2014. [PubMed: 24834056]
16. Childs EW, Tharakan B, Hunter FA, Isong M, Liggins ND. Mitochondrial complex III is involved in proapoptotic BAK-induced microvascular endothelial cell hyperpermeability. Shock 29: 636–641, 2008. [PubMed: 18414238]
17. Singleton PA, Dudek SM, Chiang ET, Garcia JG. Regulation of sphingosine 1-phosphate-induced endothelial cytoskeletal rearrangement and barrier enhancement by S1P1 receptor, PI3 kinase, Tiam1/Rac1, and alpha-actinin. FASEB J 19: 1646–1656, 2005. [PubMed: 16195373]
18. Zeng Y, Liu XH, Tarbell J, Fu B. Sphingosine 1-phosphate induced synthesis of glycocalyx on endothelial cells. Exp Cell Res 339: 90–95, 2015. [PubMed: 26364737]
19. Zhang L, Zeng M, Fan J, Tarbell JM, Curry FE, Fu BM. Sphingosine-1-phosphate Maintains Normal Vascular Permeability by Preserving Endothelial Surface Glycocalyx in Intact Microvessels. Microcirculation, 2016.
20. McVerry B, Garcia J. Endothelial cell barrier regulation by sphingosine 1-phosphate. J Cell Biochem 92: 1075–1085, 2004. [PubMed: 15258893]
21. Doggett TM, Tur JJ, Alves NG, Yuan SY, Tipparaju SM, Breslin JW. Assessment of Cardiovascular Function and Microvascular Permeability in a Conscious Rat Model of Alcohol Intoxication Combined with Hemorrhagic Shock and Resuscitation. *Methods Mol Biol* 1717: 61–81, 2018. [PubMed: 29468584]
22. Kataoka H, Ushiyama A, Kawakami H, Akimoto Y, Matsubara S, Iijima T. Fluorescent imaging of endothelial glycocalyx layer with wheat germ agglutinin using intravital microscopy. Microsc Res Tech 79: 31–37, 2016. [PubMed: 26768789]
23. Lipowsky HH, Gao L, Lescanic A. Shedding of the endothelial glycocalyx in arterioles, capillaries, and venules and its effect on capillary hemodynamics during inflammation. Am J Physiol Heart Circ Physiol 301: H2235–2245, 2011. [PubMed: 21926341]
24. Torres Filho I, Torres LN, Sondeen JL, Polykratis IA, Dubick MA. In vivo evaluation of venular glycocalyx during hemorrhagic shock in rats using intravital microscopy. Microvasc Res 85: 128–133, 2013. [PubMed: 23154280]
25. Yang X, Meegan JE, Jannaway M, Coleman DC, Yuan SY. A disintegrin and metalloproteinase 15-mediated glycocalyx shedding contributes to vascular leakage during inflammation. Cardiovasc Res, 2018.
26. Breslin JW, Wu MH, Guo M, Reynoso R, Yuan SY. Toll-like receptor 4 contributes to microvascular inflammation and barrier dysfunction in thermal injury. Shock 29: 349–355, 2008. [PubMed: 17704733]
27. Salvioli S, Ardizzoni A, Franceschi C, Cossarizza A. JC-1, but not DiOC6(3) or rhodamine 123, is a reliable fluorescent probe to assess delta psi changes in intact cells: implications for studies on mitochondrial functionality during apoptosis. FEBS Lett 411: 77–82, 1997. [PubMed: 9247146]
28. Tinsley J, Ustinova E, Xu W, Yuan S. Src-dependent, neutrophil-mediated vascular hyperpermeability and beta-catenin modification. Am J Physiol Cell Physiol 283: 51, 2002.
29. Travis AJ, Merdiushev T, Vargas LA, Jones BH, Purdon MA, Nipper RW, Galatioto J, Moss SB, Hunnicutt GR, Kopf GS. Expression and localization of caveolin-1, and the presence of membrane rafts, in mouse and Guinea pig spermatozoa. Dev Biol 240: 599–610, 2001. [PubMed: 11784086]
30. Bonitz JA, Son JY, Chandler B, Tomaio JN, Qin Y, Prescott LM, Feketeova E, Deitch EA. A sphingosine-1 phosphate agonist (FTY720) limits trauma/hemorrhagic shock-induced multiple organ dysfunction syndrome. Shock 42: 448–455, 2014. [PubMed: 25004059]
31. Wang L, Bittman R, Garcia JG, Dudek SM. Junctional complex and focal adhesion rearrangement mediates pulmonary endothelial barrier enhancement by FTY720 S-phosphonate. Microvasc Res 99: 102–109, 2015. [PubMed: 25862132]
32. Zhang XE, Adderley SP, Breslin JW. Activation of RhoA, but Not Rac1, Mediates Early Stages of S1P-Induced Endothelial Barrier Enhancement. PloS one 11: e0155490, 2016. [PubMed: 27187066]

33. Xu M, Waters CL, Hu C, Wysolmerski RB, Vincent PA, Minnear FL. Sphingosine 1-phosphate rapidly increases endothelial barrier function independently of VE-cadherin but requires cell spreading and Rho kinase. Am J Physiol Cell Physiol 293: C1309–1318, 2007. [PubMed: 17670896]

34. Haorah J, Heilman D, Knipe B, Chrastil J, Leibhart J, Ghorpade A, Miller DW, Persidsky Y. Ethanol-induced activation of myosin light chain kinase leads to dysfunction of tight junctions and blood-brain barrier compromise. Alcohol Clin Exp Res 29: 999–1009, 2005. [PubMed: 15976526]

35. Alves NG, Yuan SY, Breslin JW. Sphingosine-1-phosphate protects against brain microvascular endothelial junctional protein disorganization and barrier dysfunction caused by alcohol. *Microcirculation* In Press doi:10.1111/micc.12506, 2018.

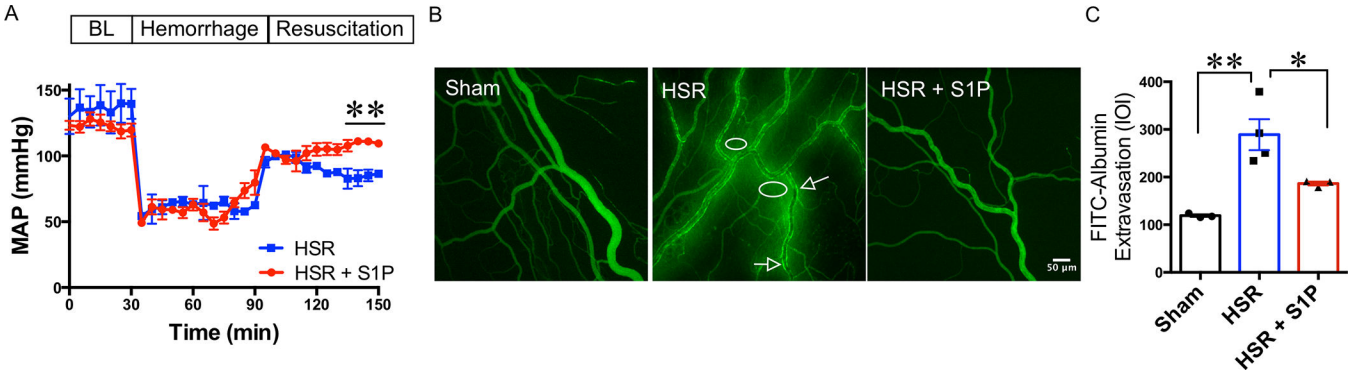


**Fig. 1.**

HSR-induced hypotension and microvascular hyperpermeability are rescued with S1P treatment. *A.* Time-course tracing of mean arterial blood pressure (MAP) of HSR (N = 3) and HSR + S1P (N = 4) rats during the fixed-pressure HSR. A 30-minute baseline measurement (BL) was taken before the start of hemorrhage. Values are shown as means ± SEM, **P < 0.01 between groups at the last three time-points of resuscitation. The groups were compared with repeated measures ANOVA and Fisher's LSD test. *B.* Representative fluorescent images of the mesenteric microvasculature of Sham (N = 3), HSR (N = 4), and HSR + S1P (N = 3) groups. Arrows indicate "hot-spots" of albumin leakage just outside the vessel wall. The circles show areas of albumin leakage into the extravascular space. *C.* Quantification of FITC-albumin extravasation was done by measuring the integrated optical intensity (IOI) in the extraluminal space adjacent to postcapillary venules. **P < 0.01, *P < 0.05 (one-way ANOVA, with Tukey's multiple comparisons test).

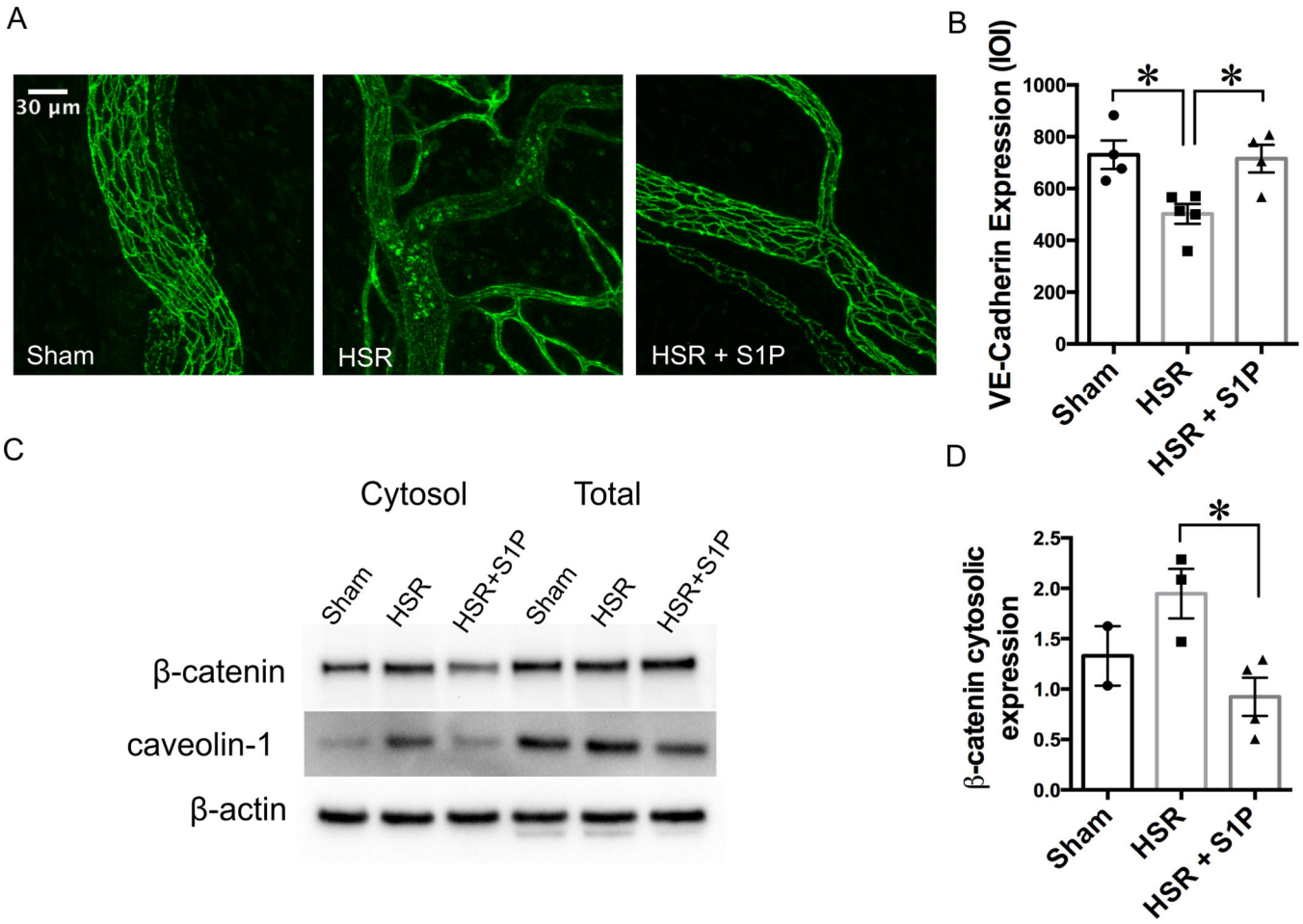


**Fig. 2.**

Resuscitation with S1P preserves adherens junction organization and expression following hemorrhage. *A.* Representative maximum intensity confocal z-projections of immunofluorescence-labeled VE-cadherin in mesenteric windows from Sham (N = 4), HSR (N = 5), and HSR + S1P (N = 4) rats. The representative images show disorganization of VE-cadherin pattern in post-capillary venules following HSR, in contrast to organized localization of VE-cadherin between endothelial cells in the sham group and HSR + S1P group. *B.* Quantification of VE-cadherin expression on the microvessels was done using the Imaris image analysis software, and is shown as integrated optical intensity (IOI) of the vessel area. At least three windows from each rat were used for quantification. *P < 0.05 (one-way ANOVA followed by Tukey's test). *C.* Western Blot showing an increase in the cytosolic concentration of β-catenin following HSR. Specific antibodies were used to determine β-catenin expression in dissected mesenteric microvessels. In the HSR + S1P group, an apparent decrease in cytosolic expression of β-catenin, with no apparent change in total protein expression was observed. Caveolin-1, a protein that is expressed on the plasma membrane of most cell types, is shown as a control for cytosolic fraction separation. These data suggest a shift in β-catenin and caveolin-1 localization during HSR. Pooled samples of microvessels isolated from 7 – 10 rats were needed for sufficient protein for analysis. *D.* Quantification of the β-catenin band intensity from multiple Western blots. The data

represent N = 2 pooled samples for sham, N = 3 pooled samples for HSR, and N = 4 pooled samples for HSR + S1P. *P < 0.05, HSR vs. HSR + S1P (unpaired t-test). The sham group was not used in the statistical analysis and is only shown for visual comparison.

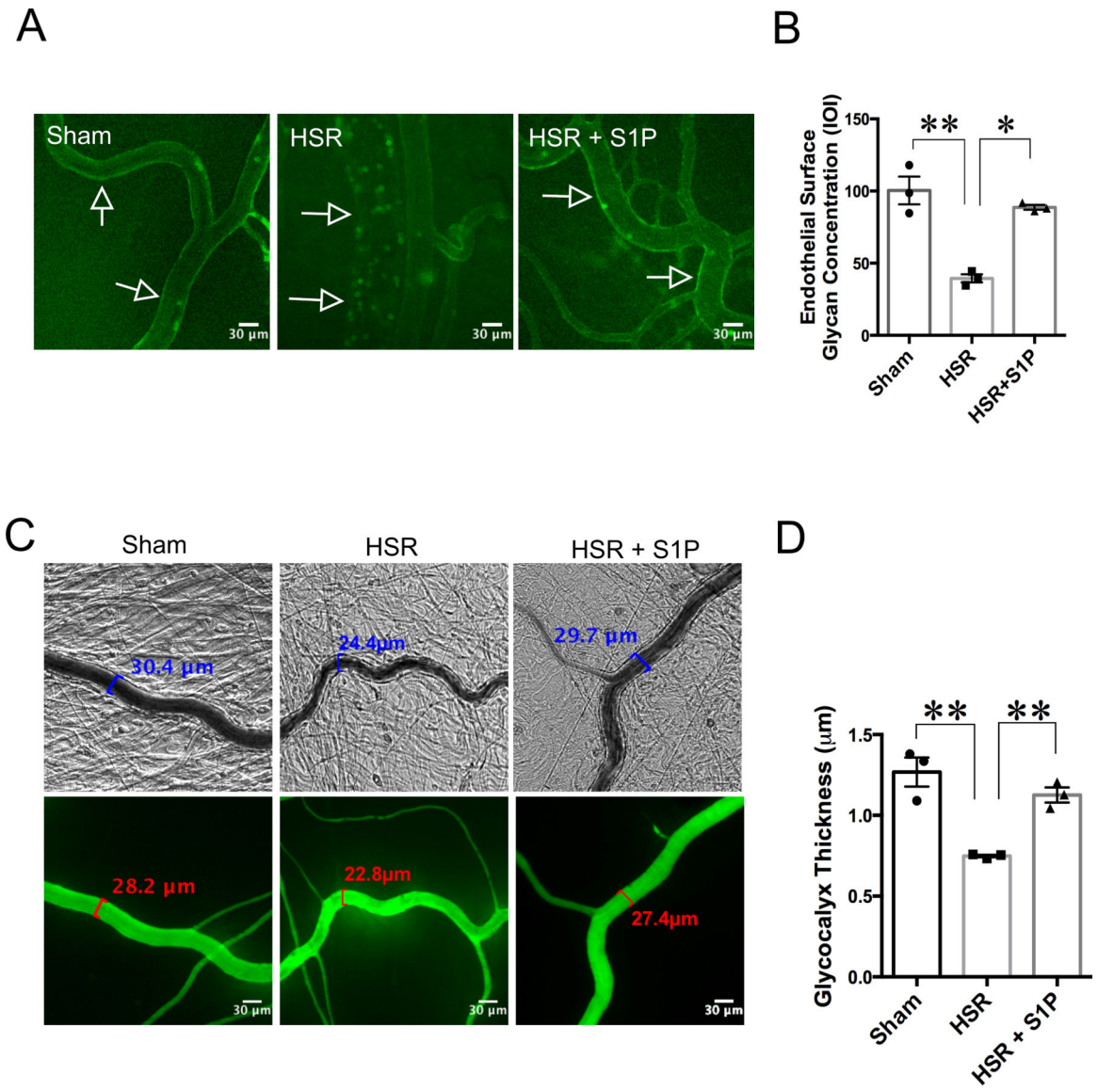


**Fig. 3.**

S1P protects the mesenteric microcirculation against glycocalyx degradation induced by HSR. *A.* Representative images showing FITC-lectin binding to the endothelial glycocalyx on the vessel walls of post-capillary venules. FITC-lectin was administered intravenously following the sham, HSR, or HSR + S1P protocols. Sham rats present high concentration of lectin bound to the venular wall, while HSR rats have much smaller amounts of FITC-lectin fluorescence. Animals that received resuscitation with S1P (HSR + S1P) retain FITC-lectin on the endothelium. *B.* Analytical quantification of FITC-lectin bound to the walls of post-capillary venules. Each data point represents the average integrated optical intensity (IOI) of at least 3 separate vessels in one rat. **P < 0.01, *P < 0.05 for the indicated groups, one-way ANOVA followed by Tukey's multiple comparisons test. N=3 rats in each group. *C.* Measurement of rat mesenteric microvascular glycocalyx thickness using FITC-dextran (150 kDa) exclusion assay was performed withe brightfield and fluorescent images of mesenteric venules. *D.* Quantification of glycocalyx thickness from the imaging data is shown. Each

data point represents the average of glycocalyx measurements on 4 – 8 areas per rat. **P < 0.01, one-way ANOVA, with Tukey's multiple comparisons test. N = 3 rats per group.

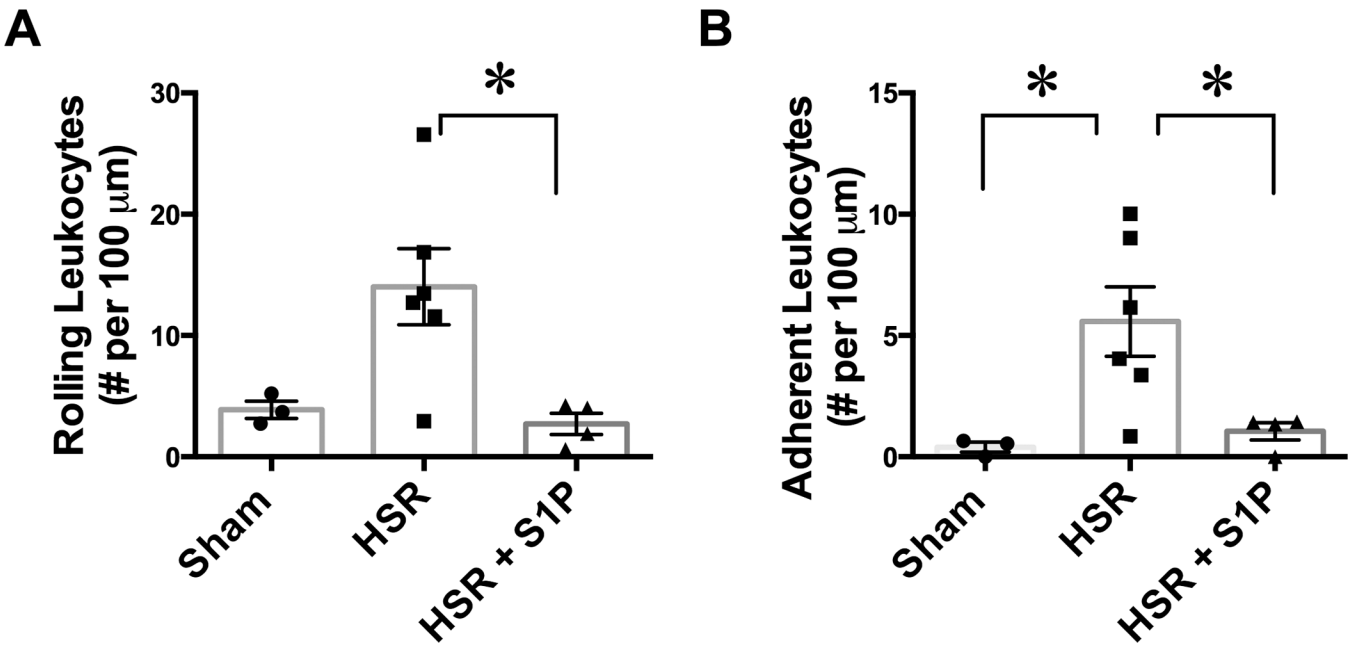


**Fig. 4.**

Resuscitation with S1P decreases leukocyte-endothelium interactions following hemorrhage. *A.* S1P administration during resuscitation after hemorrhage significantly reduces the number of slow-rolling leukocytes in mesenteric postcapillary venules, compared to HSR alone. *B.* The number of leukocytes firmly adhered to the endothelium following HSR is significantly higher than sham control rats. Resuscitation with S1P significantly decreases firm leukocyte adhesion. *P < 0.05 (one-way ANOVA, with Tukey's multiple comparisons test) for the indicated groups. Sham group, N = 3; HSR, N = 6; HSR + S1P, N = 4.

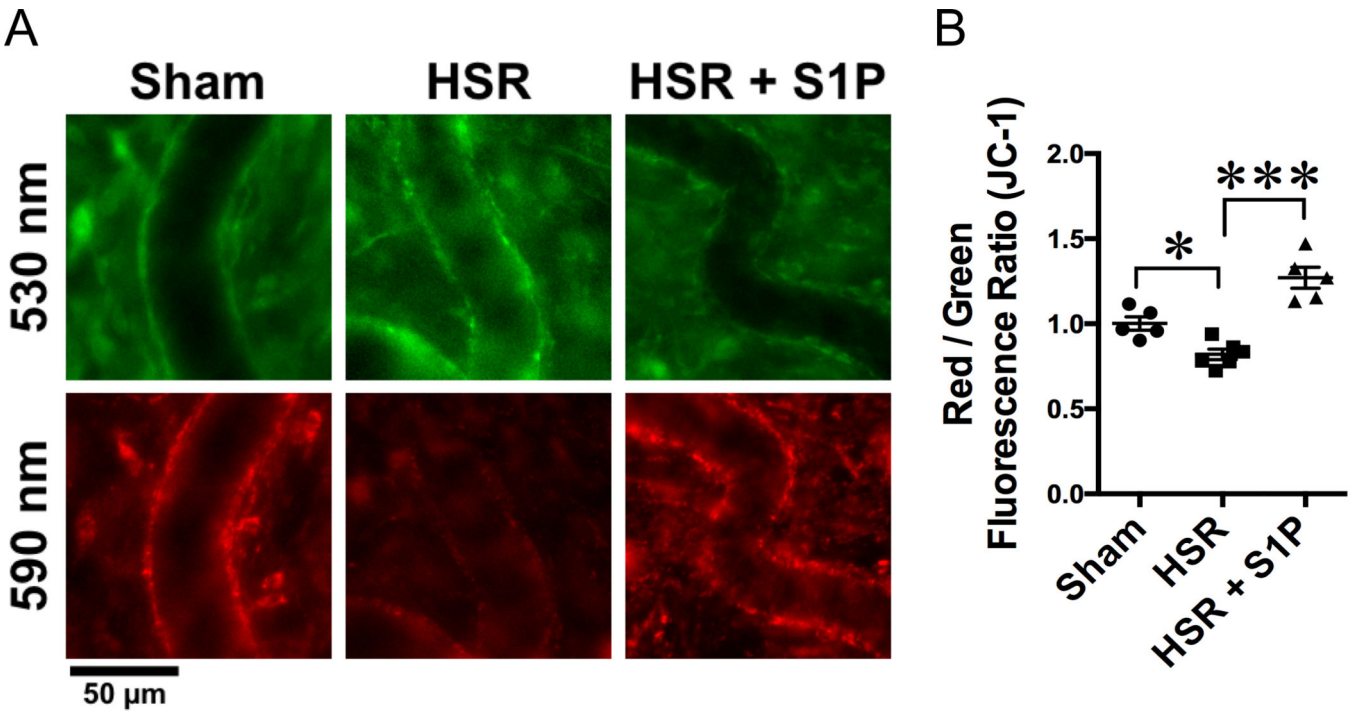


**Fig. 5.**

S1P protects against HSR-induced mitochondrial dysfunction. *A.* Representative *in vivo* IVM of mesenteric windows from the sham, HSR and HSR + S1P groups. In sham rats, JC-1 aggregated in the mitochondria of post-capillary venules and fluoresced red (590 nm images), indicating healthy mitochondria. HSR rats show impaired mitochondrial membrane integrity, causing elevated diffusion of JC-1 to the cytoplasm (green fluorescence, 530 nm images) and decreased red aggregate. S1P-treated rats show intact mitochondria as JC-1 red aggregate. *B.* Analysis of red to green fluorescence ratio in the walls of post-capillary venules show that HSR causes significant mitochondrial depolarization, which is rescued by resuscitation with S1P. *P < 0.05, ***P < 0.01. The groups were compared with one-way ANOVA and Tukey's multiple comparisons test. Sham, N = 5; HSR N = 6; HSR + S1P, N = 5.

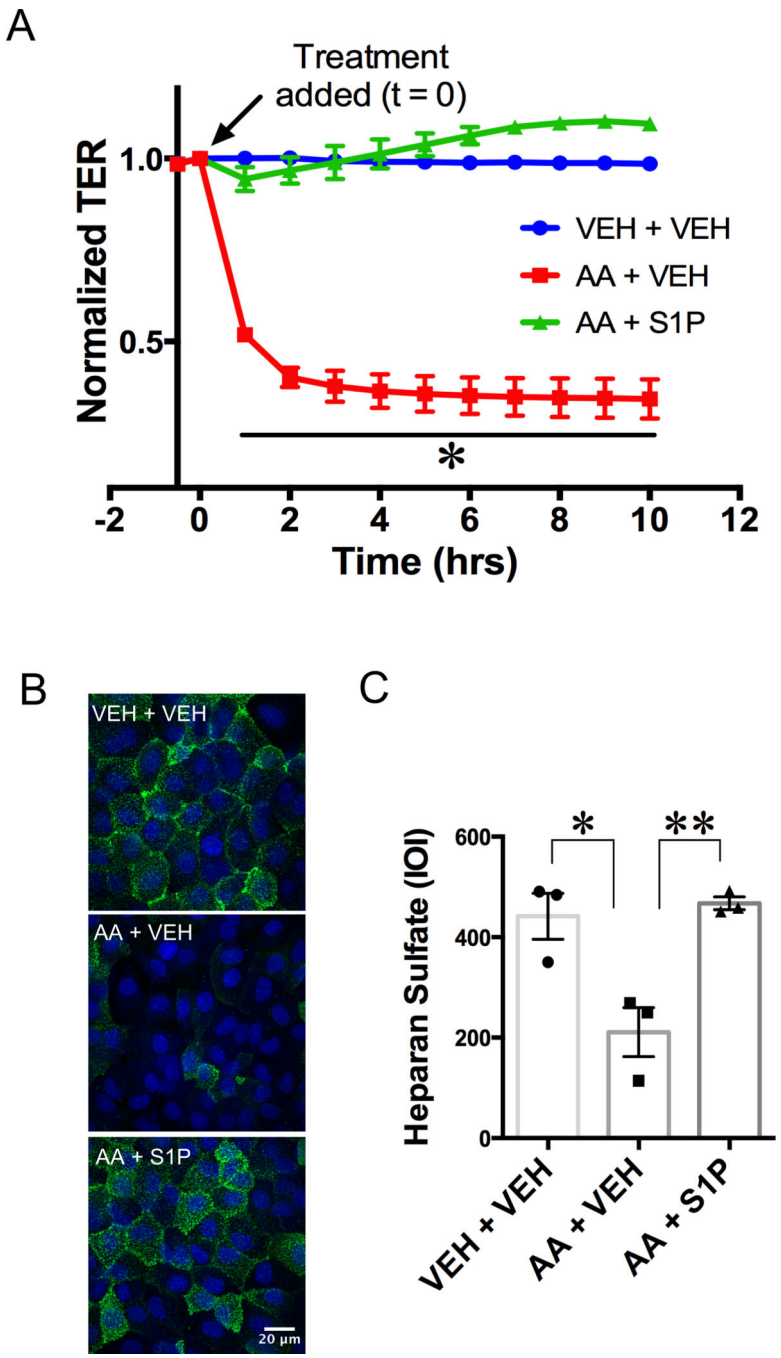


**Fig. 6.**

S1P rescues endothelial barrier dysfunction and glycocalyx degradation induced by inhibition of mitochondrial complex III. *A*. Dynamic changes in TER of RIMEC monolayers treated with vehicle control (bECM) followed by vehicle (VEH + VEH), antimycin-A followed by vehicle (AA + VEH) and AA followed by S1P (AA + S1P). RIMEC treated with antimycin-A (AA) display a time-dependent decrease in TER, which is rescued by treatment with S1P. Tracings indicate the mean resistance normalized to $t = 0$ (indicated by arrow) ± S.E. for each hour following treatment. N = 5 independent

experiments, with 4 – 8 monolayers per group in each experiment. Statistical analysis of normalized TER was done with repeated-measures ANOVA, with Tukey's multiple comparisons test, *P < 0.05. *B.* Representative z-projections of confocal immunofluorescence images of the glycocalyx component heparan sulfate. High expression of heparan sulfate can be seen on RIMECs treated with vehicle only (VEH + VEH). Lower heparan sulfate fluorescence is seen in cells treated with AA + Vehicle. Cells treated with S1P show high heparan sulfate fluorescence (AA + S1P). *C.* Quantification of heparan sulfate fluorescence on RIMEC show a significant decrease induced by AA that is rescued by S1P treatment. Heparan sulfate expression is expressed as the mean integrated optical intensity (IOI) from three independent experiments. ***P < 0.001 (one-way ANOVA, Tukey's multiple comparisons test).

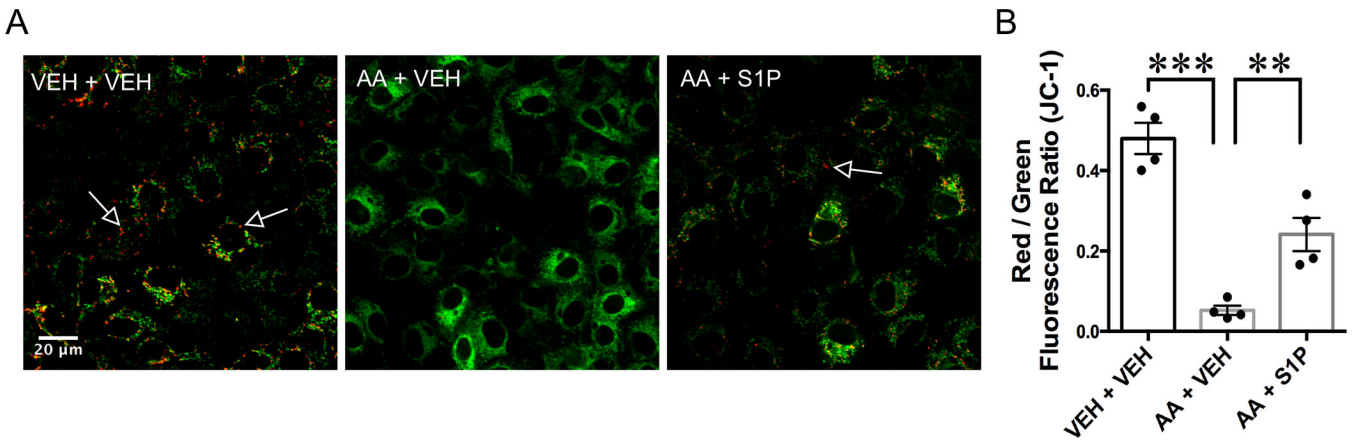


**Fig. 7.**

S1P protects endothelial cells from mitochondrial depolarization induced by inhibition of complex III. *A.* Representative confocal fluorescence images of JC-1-loaded RIMECs treated with antimycin-A (AA) followed by S1P or vehicle. Control cells (VEH + VEH) show JC-1 aggregates (red fluorescence, indicated by arrows) in the mitochondria, indicating healthy mitochondria. Cells treated with AA show an increase in cytoplasmic JC-1 monomer (green fluorescence), indicating mitochondrial depolarization. Cells treated with S1P after antimycin-A (AA + S1P) show some intact mitochondria. *B,* Quantification of mitochondrial depolarization is shown in terms of Red/Green fluorescence ratio. AA treatment causes a significant decrease in red to green fluorescence compared to controls. AA treatment followed by S1P significantly increases red to green fluorescence ratio on RIMECs, indicating protection of complex III by S1P. All images were acquired 10 minutes after addition of S1P or vehicle. *P < 0.05, **P < 0.01, one-way ANOVA, followed by Tukey's multiple comparisons test. N=4 experiments for each group, with at least four cells analyzed in each independent experiment.